Research Article | Vol. 28, No. 5 / 2 March 2020 / Optics Express 6766
Optics EXPRESS

Routing of strongly confined terahertz spoof surface plasmon polaritons on metasurfaces along straight and curved pathways with subwavelength width

SVEN BECKER,* TASSILO FIP, AND MARCO RAHM

Department of Electrical and Computer Engineering and Research Center OPTIMAS Technische University Kaiserslautern, Kaiserslautern, Germany
**svbecker@eit.uni-kl.de*

Abstract: In search of new technologies for optimizing the performance and space requirements of electronic and optical micro-circuits, the concept of spoof surface plasmon polaritons (SSPPs) has come to the fore of research in recent years. Due to the ability of SSPPs to confine and guide the energy of electromagnetic waves in a subwavelength space below the diffraction limit, SSPPs deliver all the tools to implement integrated circuits with a high integration rate. However, in order to guide SSPPs in the terahertz frequency range, it is necessary to carefully design metasurfaces that allow one to manipulate the spatio-temporal and spectral properties of the SSPPs at will. Here, we propose a specifically designed cut-wire metasurface that sustains strongly confined SSPP modes at terahertz frequencies. As we show by numerical simulations and also prove in experimental measurements, the proposed metasurface can tightly guide SSPPs on straight and curved pathways while maintaining their subwavelength field confinement perpendicular to the surface. Furthermore, we investigate the dependence of the spatio-temporal and spectral properties of the SSPP modes on the width of the metasurface lanes that can be composed of one, two or three cut-wires in the transverse direction. Our investigations deliver new insights into downsizing effects of guiding structures for SSPPs.

1. Introduction

Modern electronic devices contain a variety of miniaturized sensors and signal processing units that are based on integrated circuit technologies. The perpetual demand for downsizing such microsystems and the integration of several applications in one small chip has garnered an increasing interest into the field of plasmonics in recent years, especially into the topic of surface plasmon polaritons (SPPs). SPPs are electromagnetic surface waves that can propagate along metal surfaces provoked by the coupling of photons and free charges at the interface between the metal and its surrounding media [1]. Due to their strong field confinement to metal surfaces and their ability of breaking the diffraction limit, SPPs can be tightly guided on compact signal pathways without significant attenuation [2–4] and are the signals of choice for use in highly sensitive surface sensors [5–8]. While strongly confined SPPs on smooth metal surfaces only exist at optical frequencies, artificially manufactured metasurfaces are required to mimic SPP characteristics at microwave or terahertz (THz) frequencies [9]. These surface waves with emulated SPP characteristics are called spoof surface plasmon polaritons (SSPPs) [10]. Various metasurface structures that enable SSPP modes, such as planar metamaterials composed by split-ring-resonators [11–13], H-shaped patches [14–16] or similar metallic patterns [17–25] as well as corrugated metal surfaces with grooves and pillars [6,7,26–33], were proposed in recent years. While metasurfaces composed of ultrathin metallic patterns can be directly processed on printed circuit boards (PCBs) or can be manufactured by straight forward fabrication techniques, corrugated metal surfaces with groove depths of up to several hundred micrometers cannot

#384725 https://doi.org/10.1364/OE.384725
Journal © 2020 Received 29 Nov 2019; revised 30 Jan 2020; accepted 3 Feb 2020; published 21 Feb 2020

Optics EXPRESS

lean on easy technologies and require more sophisticated fabrication methods. Furthermore, corrugated metal surfaces only provide limited means for manipulating the spatio-temporal and spectral properties of SSPPs, for which reason we focus on the investigation and realization of ultrathin metallic metasurfaces. While these metasurfaces provide favorable properties in a manifold context, past reports in the literature only focused on the demonstration of very few aspects as they mostly investigate the propagation of SSPPs along straight pathways. Frequently, the SSPPs are well bound in the direction perpendicular to the surface, yet are completely unconfined in the plane in which they propagate [11–13,16–18]. In highly integrated circuits however, it is mandatory that the metasurface structures also confine the SSPPs within the plane of propagation on a subwavelength scale and allow deliberate waveguiding and routing of the SSPPs on pathways with subwavelength path width. In this context, latest research that covers such flat and compact sized metasurface structures at terahertz frequencies lack experimental evaluation [20–22]. They are either restricted to numerical simulation models [20,22] or they only deliver simple proof-in-principle demonstrations in the microwave regime [21]. For this reason, it was our goal to design and fabricate ultrathin metasurfaces with tailored dispersion to gain full control over the in-plane propagation of terahertz SSPPs, while still maintaining a subwavelength field confinement to the metasurface. Furthermore, we applied the electro-optic sampling (EOS) measurement technique to examine the spatio-temporal properties of a terahertz SSPP mode on fabricated metasurfaces. The proposed metasurfaces are composed of a periodic arrangement of cut-wires on a dielectric, flexible thin-film substrate. As we show by numerical simulations and experimentally prove by near-field mapping of the propagating SSPPs, the SSPPs display a subwavelength out-of-plane confinement as well as a strong in-plane confinement with respect to the plane of propagation. In addition to the out-of-plane and in-plane confinement, the metasurface can control the in-plane propagation pathways of the SSPPs. To give specific examples, we designed metasurfaces that guide the SSPPs on straight and curved routes with a propagation length of several millimeters. Focusing on the maximization of the in-plane confinement of the SSPPs, we investigated the impact of an increasing in-plane confinement on the dispersion of the propagating SSPP mode. In our study, we limited the width of the metasurface pathway to a small number of cut-wire unit cells and found that the number of unit cells transverse to the propagation direction of the surface waves has a strong influence on the spectral bandwidth of the supported SSPP mode.

2. Dispersion characteristics of the cut-wire metasurface

In this section, we theoretically study the impact of transverse pathway boundaries on the spectral dispersion of SSPPs on metasurfaces. For this purpose, we investigate cut-wire metasurfaces with three different path widths. As can be seen in Fig. 1, the metasurfaces are either composed of a single row (Fig. 1(a)), two rows (Fig. 1(b)) or three rows of cut-wires (Fig. 1(c)) in the direction transverse to the propagation path of the SSPPs. The cut-wires build the unit cells of the investigated metasurfaces and must be specifically designed and spatially arranged to support SSPP modes. In addition to SSPP propagation along straight pathways, we study the spatio-temporal and spectral properties of SSPPs that travel on a curved course. As depicted in Fig. 1(d), the boundaries of the curve are set by the cut-wires that compose the metasurface. In our case, the transverse width of the curved path is equivalent to 3 unit cells. In the following, we refer to these four different types of metasurfaces as the straight 1-cut-wire, 2-cut-wire and 3-cut-wire metasurface as well as the curved 3-cut-wire metasurface.

In a first step, we numerically calculated the spectral dispersion of the SSPPs by use of the eigenmode solver of CST Microwave Studio. Figure 2(a) shows the simulated metasurface unit cell that consists of a metallic cut-wire on a dielectric substrate. In the eigenmode calculations, the cut-wire is treated as a perfect electric conductor (PEC) and the substrate material is a loss-free dielectric thin film with a relative permittivity of $\epsilon_r = 2.3$. In this context, the use of a

Optics EXPRESS

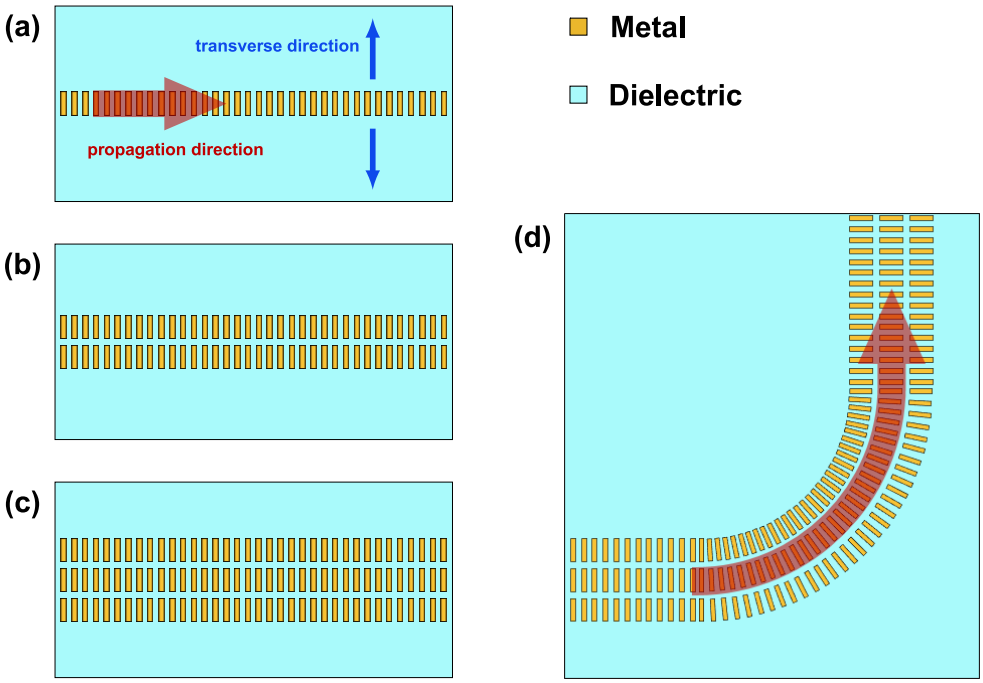

Fig. 1. Schematic top view of the investigated cut-wire metasurfaces. (a) - (c) Cut-wire metasurfaces with a straight pathway. The metasurface pathways are spatially limited in transverse direction by (a) one ,(b) two and (c) three cut-wires. (d) Curved metasurface pathway for in-plane surface wave routing.

thin-film dielectric, be it loss-free or lossy, restricts the number of unwanted substrate guided modes that can occur in addition to the desired SSPP modes [13]. The calculation domain is terminated by periodic boundaries in x -and y-direction as well as electric boundaries with added free space in z-direction. For the simulation of metasurfaces with limited spatial extension in the y-direction, sufficient space is allowed between the dielectric substrate and the boundaries in y-direction to avoid coupling between the electromagnetic fields in the unit cell and their periodic image fields, as illustrated in Fig. 2(b). We found by means of a parametric study that a distance of 3000 µm between the cut-wires and the periodic boundaries in y-direction was sufficient to avoid coupling between the actual metasurface and its images, which enabled us to simulate metasurfaces of limited path width.

By sweeping the phase difference $\Delta\theta$ of the electromagnetic fields at the opposite boundaries in x-direction from 0° and 180°, the eigenmode solver calculates the eigenfrequencies of the SSPPs on the metasurface within the first Brillouin zone. With the relation $k_x = (2\pi\ \Delta\theta)/(w_s\ 360°)$, we determined the dependence of the SSPP eigenfrequencies on the x-component of the wavenumber k_x to obtain the dispersion relation of the metasurface. In Fig. 3(a), the spectral dispersion curves of the fundamental mode of the SSPPs on the straight 1-cut-wire (1), 2-cut-wire (2) and 3-cut-wire metasurface (3) are shown in relation to the light lines of free space (black dashed) and of the dielectric substrate (blue dashed). On all three metasurfaces, the spectral dispersion curve of the considered SSPP mode converges asymptotically to a common high cut-off frequency of 0.68 THz for increasing wavenumber k_x. For convergence studies, we also numerically calculated the dispersion of the SSPPs on a metasurface path that consists of an infinite number of identical cut-wire unit cells transverse to the propagation direction of the SSPPs. The calculated dispersion

Optics EXPRESS

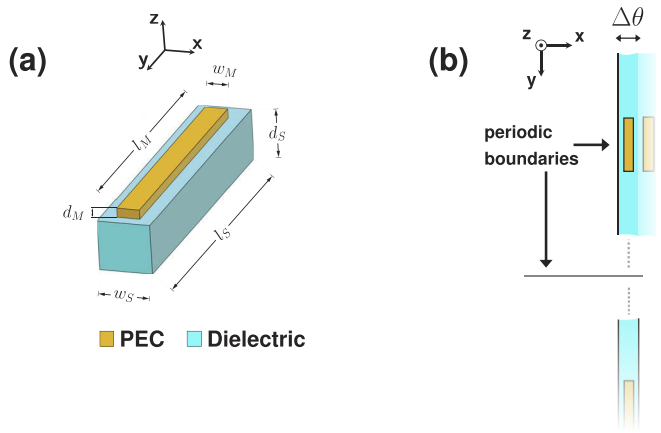

Fig. 2. (a) Metsasurface unit cell. The geometric parameters are l_S = 170 µm, w_S = 10 µm, d_S = 50 µm, l_M = 165 µm, w_M = 5 µm and d_M = 0.3 µm. (b) Periodic continuation of the unit cell as a consequence of periodic boundaries in x- and y-direction. $\Delta\theta$ is the phase difference of the electromagnetic fields calculated from the phase of the fields at the location of the opposing boundaries in x-direction.

curve is shown as case (4) in Fig. 3(a). As expected, the high cut-off frequency of the SSPPs remains at 0.68 THz. We found that the high cut-off frequency strongly depends on the geometry of the unit cells. To support this claim, we calculated the dispersion of SSPPs on a metasurface path, whose width is defined by a single cut-wire with a length of l_M = 505 µm. Hereby, the cut-wire length is chosen to be equal to the path width of the 3-cut-wire metasurface in case (3). As shown in case (5) of Fig. 3(a,) the dispersion of the SSPPs converges asymptotically to a high cut-off frequency of 0.23 THz that significantly differs from the high cut-off frequency in cases (1)-(4).

As the study of cases (1)-(4) reveals, the path width, that is governed by the number of unit cells in the direction transverse to the propagation direction of the SSPPs, defines the slope of the spectral dispersion curve. The latter property becomes even more obvious, when we zoom into the spectral dispersion diagram, as shown in Fig. 3(b). The dispersion slope decreases for increasing number of unit cells in the transverse direction of the metasurface path and converges for an infinite number of unit cells, as in case (4). Figure 3(b) also evidences that the slope of the spectral dispersion defines the frequency and the wavenumber at which the dispersion curve intersects the light line of the substrate, which implies that this intersection point is dependent on the metasurface path width. Since a SSPP mode is only confined to the metasurface, when its phase velocity on the surface is slower than the phase velocity it would have in the surrounding medium, in our case air or a dielectric, the frequencies at the intersection points define the low cut-off frequency of the corresponding SSPP mode. For frequencies above the low cut-off frequency, SSPPs are confined to the metasurface and for increasing frequency their spatial confinement asymptotically approaches its maximum for the high cut-off frequency. In other words, the SSPPs enter a subwavelength regime above the low cut-off frequency and their electromagnetic energy is confined beyond the diffraction limit of freely propagating waves. From the spectral dispersion diagram of Fig. 3(b), we determined a low cut-off frequency of 0.48 THz , 0.34 THz and 0.28 THz and 0.18 THz for the straight 1-, 2- and 3-cut-wire metasurface and for the metasurface with an infinite number of identical cut-wires along the path width. This implies that the low cut-off frequency of the considered SSPP mode increases for decreasing path width, when the geometry of the unit cell is identical for all path widths. Since, under the same conditions, the high cut-off frequency remains unaffected by the path width, we conclude

Optics EXPRESS

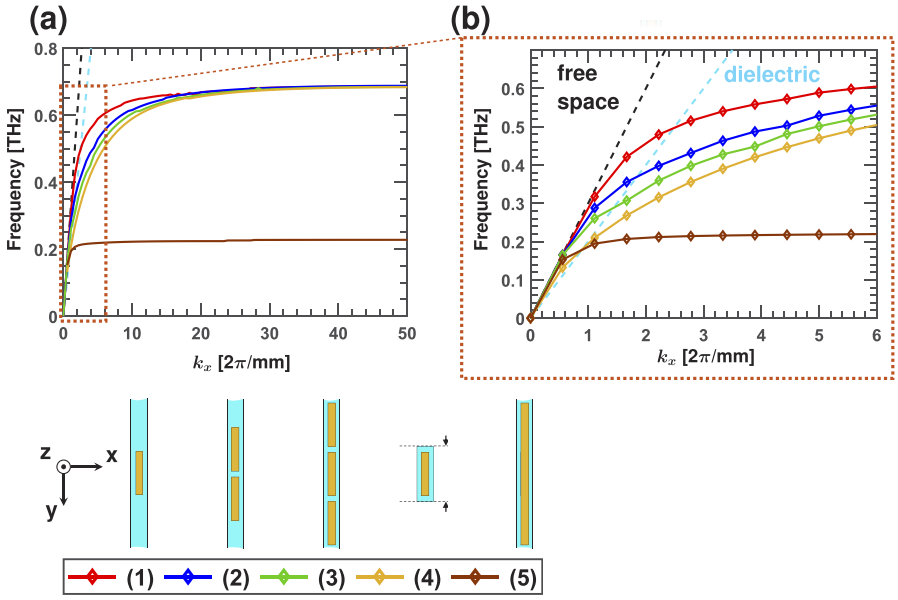

Fig. 3. (a) Dispersion relation of the SSPPs on a straight (1) 1-cut-wire (2) 2-cut-wire, (3) 3-cut-wire metasurface and (4) on a metasurface with an infinite number of identical cut-wires in the direction transverse to the propagation direction of the SSPPs. (5) Dispersion relation of a straight 1-cut-wire metasurface with a path width of l_M = 505 µm that is identical to the path width of the 3-cut-wire metasurface in (3). (b) Zoom of the dispersion diagram of (a) for better distinction between the different dispersion curves. The light lines of free space and of the dielectric substrate are plotted as dashed lines in black and blue. The simulated metasurface structures and the corresponding legend for the two diagrams are shown below.

that confining the path width of the metasurface automatically limits the spectral bandwidth of the considered SSPP mode.

For studies of the spatial distribution of the electric field of the propagating SSPP mode, we numerically simulated the propagation of the SSPP on a straight 1-cut-wire, 2-cut-wire and 3-cut-wire metasurface with each a length of 4 mm. In the simulation model, we excited the SSPP mode via diffraction on a metal edge in the vicinity of the metasurface structure, as depicted in Fig. 4(a). Note that we applied open boundaries for the full wave simulation. Since the eigenmode solutions indicated TE-polarized SSPPs, the edge coupling requires an excitation beam with polarization in y-direction. As an example, Fig. 4(b) depicts the y-component of the electric field E_y for a propagating SSPP mode at a frequency of 0.28 THz in a cross-sectional plane of the 3-cut-wire metasurface. The existence of SSPP propagation is evidenced by the strong field enhancement and field confinement near the metasurface. Beside the strongly confined fields of the SSPP mode, we also observe scattered fields that can be attributed to the residual fraction of the excitation waves that are not coupled into the SSPP mode. These fractions are either scattered into free space or diffracted into the substrate. We also noticed significant reflection of the SSPPs at the path end, which indicates that the propagation length of the SSPP mode exceeds the simulated path length of 4 mm. Furthermore, the SSPP mode displays specific spatial properties in the z-component of the electric field E_z. This is emphasized in Fig. 5, where the real part of E_z is plotted on the xy-cross-sectional plane 50µm above the straight 1-cut-wire (Fig. 5(a)), 2-cut-wire (Fig. 5(b)) and 3-cut-wire metasurface (Fig. 5(c)) at the low cut-off frequency of 0.48 THz, 0.34 THz, 0.28 THz, respectively. Additionally, the corresponding close-ups of the field

Optics EXPRESS

plots clarify the geometric relation between the electric field distribution of the SSPPs and the subjacent metasurface structure. From the spatial distribution of E_z, we conclude that the SSPP propagates in an odd transverse mode as the phase of the two field maxima in the transverse direction is 180° out of phase. We can easily distinguish the odd SSPP mode for the E_z-field from the residual scattering fields of the excitation wave and from undesirable guided modes in the substrate, since those modes only occur as even modes. We also observe that the electric field distribution is spatially spread, when the path width is increased from one to three unit cells, while the odd phase characteristics of the SSPP mode is conserved. The spatial spreading of the electric field distribution becomes even more obvious, when we plot the absolute value of E_z along an intersection line in y-direction at x = 1000 µm. According to Fig. 5(d), the spatial distance between the two field maxima of the odd mode increases for increasing number of metasurface unit-cells from one cut-wire (1) to three cut-wires (3). Furthermore, the electric field exponentially decays at the boundaries of the metasurface , thus indicating a strong in-plane field confinement of the SSPP mode within the path width of the metasurface.

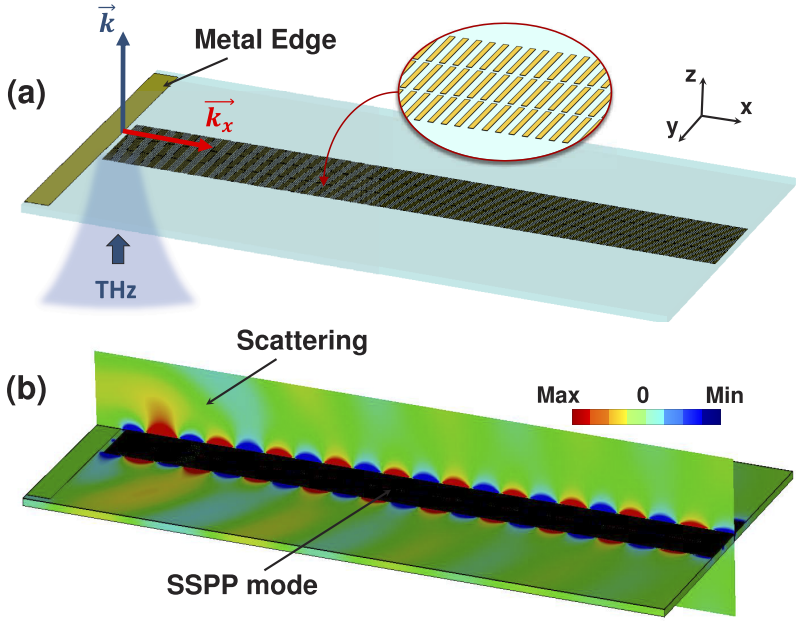

Fig. 4. (a) Simulation model of a 4mm long 3-cut-wire metasurface with straight pathway. The terahertz wave, that is incident from the direction of the substrate, is coupled to the SSPP mode by edge diffraction from a metal edge. (b) Real part of the the y-component of the scattered electric field E_y from the metal edge in the coupling region together with the real part of the y-component of the propagating SSPP electric field in the propagation region at a frequency of 0.28 THz.

Optics EXPRESS

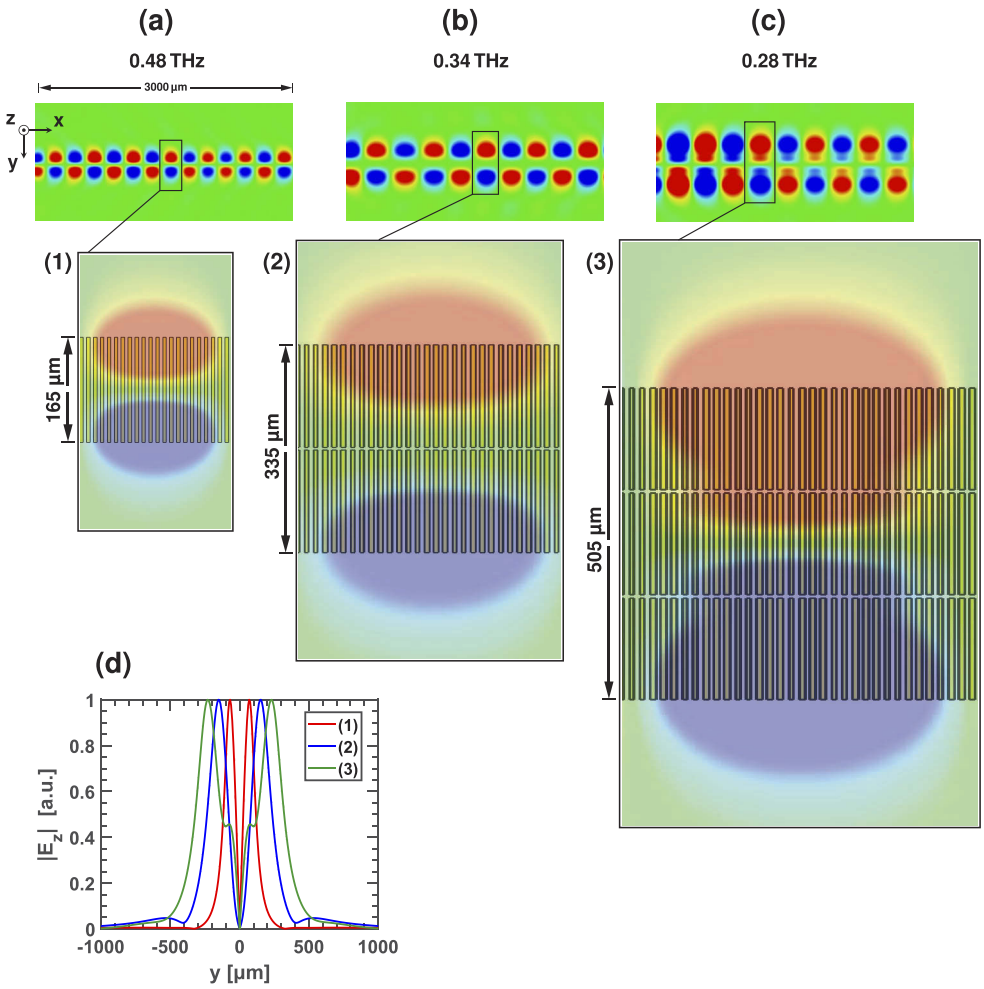

Fig. 5. Field maps of the z-component of the SSPP electric field E_z in the x-y-plane at z = 50µm away from the metasurface. The close-ups indicate the geometric relation between the SSPP electric field distribution and the subjacent metasurface structure. The SSPP electric field is monitored at frequencies of (a) 0.48 THz for the straight 1-cut-wire metasurface, (b) 0.34 THz for the 2-cut-wire metasurface and (c) 0.28 THz for the 3-cut-wire metasurface. (d) Absolute value of Ez along an intersection line in y-direction at x = 1000 µm transverse to the propagation direction of the SSPPs for (1) the 1-cut-wire, (2) the 2-cut-wire and (3) the 3-cut-wire metasurface.

3. Near-field spectroscope and metasurface fabrication

In order to verify the existence of SSPPs with tight surface binding and strong confinement transverse to the propagation direction on the designed straight and curved 1-, 2- and 3-cut-wire-metasurfaces, we imaged the temporal dynamics of the electric near-field amplitude and phase of the SSPPs via electro-optical sampling (EOS) in reflection geometry, as depicted in Fig. 6. With an EOS-crystal mounted on a three-dimensional positioning stage, we raster scanned the time trace of the electric near-field at an approximate distance of 50 µm to the metasurface. As an example for the spatio-temporal dynamics of the SSPP near-field, two measured terahertz pulse time traces are illustrated in the right graph of Fig. 6. The time signals were extracted from the

Optics EXPRESS

spatio-temporal measurement of the SSPP near-field at a distance of 50 µm from the straight 3-cut-wire-metasurface. The red line corresponds to the terahertz pulse that was measured at the excitation point of the SSPP, i.e. close to the incoupling metal edge. Likewise, the blue line refers to the measured terahertz pulse after propagation over a distance of 1.5 mm from the excitation point. The dispersion of the terahertz pulse indicates a propagating mode, whose spectral properties can be derived by Fourier transform. By measurement of the terahertz time traces for each scanning point, we obtain full information over the spatio-temporal dynamics of the SSPPs on the metasurface. For the EOS measurement, we used a (100)-cut GaP crystal with a thickness of of 250 µm and an aperture of 4mm x 4mm. Due to its (100)-cut, the EOS crystal was only sensitive to the out-of-plane component E_z of the electric terahertz field, which allowed us to study the spatio-temporal and spectral characteristics of the SSPP mode under the same conditions as were presumed in the theoretical considerations of the previous section. For further information on the terahertz near-field time-domain spectrometer, the reader is referred to [34].

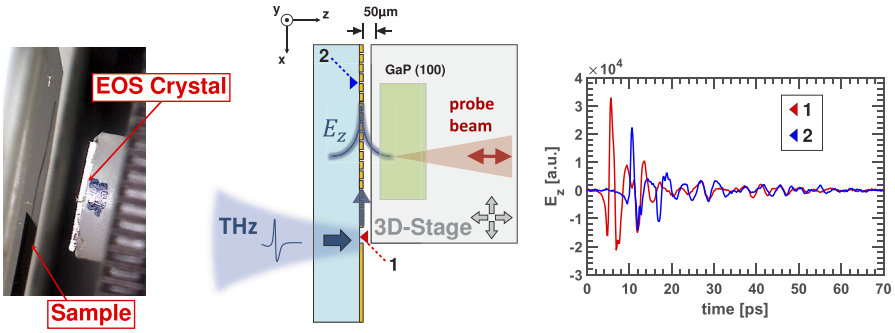

Fig. 6. Schematic view of the EOS near-field sampling. The EOS crystal, which is a GaP-crystal with a (100)-cut, is mounted on a three-dimensional (3D) positioning stage. The (100)-cut GaP is only sensitive to the out-of-plane component E_z of the THz electric field. The EOS-crystal raster scans the terahertz near-field at an approximate distance of 50 µm from the metasurface, while the sample is illuminated by the THz signal on the unstructured side. A linearly polarized optical probe beam is focused onto the EOS crystal facet that faces the metasurface. Via the electro-optic effect, the polarization of the probe beam is rotated by the influence of the SSPP electric near-field. Based on the polarization rotation, the electric field amplitude and phase of the SSPPs can be determined. The graph on the right shows two terahertz pulse time traces of the detected THz signal, one recorded at the excitation point of the SSPP (red) and the other after SSPP propagation over a distance of 1,5 mm away from the excitation point (blue).

We fabricated the metasurfaces with the straight and curved pathways by means of standard photolithography in the cleanroom facilities of the Nano Structuring Center (NSC) at the Technische University Kaiserslautern. An example of a microscope picture of a 3-wire metasurface along a curved pathway is shown in Fig. 7(a). We used a ZeonorFilm ZF-16 Series thin-film polymer with a thickness of 50µm as a substrate for all fabricated metasurfaces, as shown in Fig. 7(b). The dielectric properties of Zeonor were also taken into account in the preceding numerical calculations, which ensures a direct comparability between the experimental investigation and the theoretical studies. We metalized the surface of the thin film substrate via electron beam evaporation with a layer sequence of 0.01µm of Cr and 0,3µm of Au, as depicted in Fig. 7(c). After lift-off, we obtained metasurfaces along straight and curved pathways that were composed of cut-wires with a length of about 164 µm and a separation distance of about 4.5 µm (see Fig. 7(d)). For edge coupling of free terahertz waves into SSPP surface modes, we processed a metal patch on top of the metasurfaces according to Fig. 7(e).

Optics EXPRESS

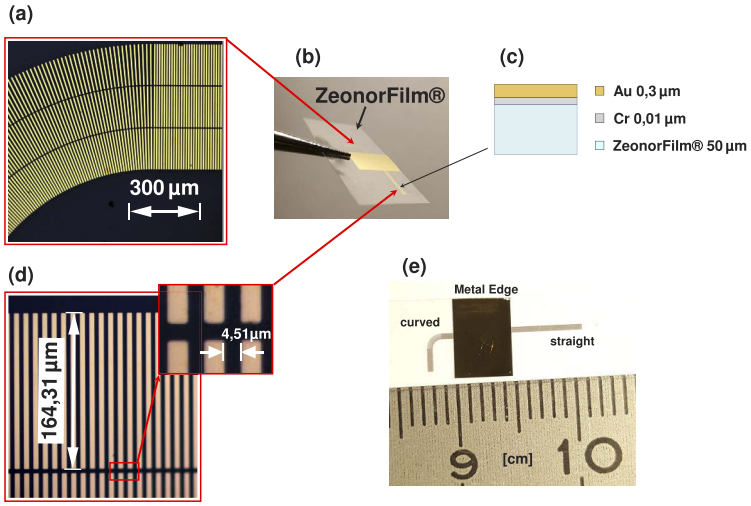

Fig. 7. (a) Microscope image of a 3-cut-wire metasurface along a curved pathway. (b) ZeonorFilm as dielectric substrate, (c) The metasurfaces are composed of 0.01µm of Cr and 0,3µm of Au. (d) Microscope image of an excerpt of a cut-wire metasurface with a cut-wire length of 164µm and a cut-wire separation of 4.5 µm. (e) Metal edge for coupling of free terahertz waves into SSPP modes. The ruler visualizes the size of the metasurface pathways and the size of the metal edge.

4. Measurement of the electric near-field of the SSPPs

For the measurement of the electric near-field of the terahertz SSPPs, we raster scanned the fields with an EOS crystal at a distance of about 50 µm parallel to the metasurface. With this method, we were able to obtain a 2-D map of the amplitude and phase of the electric field of the terahertz SSPPs in the scan plane with a spatial resolution of 50µm x 50µm. Since we measure the time trace of the electric field amplitude and phase for each scan point, we obtain spectral information about the electric field of the SSPP for frequencies between 0.1 THz and 1 THz in a single scan. In consequence, this enables us to draw direct comparisons between the electric field of the SSPPs at different frequencies. For the visualization of the SSPP near-field, we plotted the real part of the measured electric field at the considered frequency as a 2-D color map. Note that we applied a low-cut filter in the spatial frequency regime to eliminate residues of the terahertz waves that were not edge-coupled into the investigated SSPP modes and thus were directly transmitted through the metasurface into the EOS crystal. Furthermore, we cut off high frequency noise in the measurement data.

The measured spatial distribution of the electric SSPP fields on a straight 1-, 2-, and 3-cut-wire metasurface is shown in Fig. 8(a), Fig. 8(b) and Fig. 8(c), respectively. Each figure contains a microscope image of the investigated metasurface in the top row and the 2-D color maps of the measured SSPP near-field at two different frequencies in the two mid rows. The plots at the bottom depict a comparison between the experimentally measured absolute electric field along an intersection line in y-direction at constant x-location and the numerically simulated profile of the field distribution, which we have already shown in Fig. 5(d). We first discuss the spatial distribution of the measured SSPP mode on the straight 1-cut-wire metasurface in Fig. 8(a), measured at frequencies of 0.48 THz and 0.54 THz. At a frequency of 0.48 THz, we observe a strong electric field enhancement in the area around y = 1000µm, which corresponds to the location of the 1-cut-wire metasurface. The SSPP propagates in x-direction in an anti-symmetric, odd-phase mode, as can be identified by the 180° phase difference between the electric near-field

Optics EXPRESS

above and below the axis through y = 1000µm parallel to the x-axis. Furthermore, the SSPP mode is spatially confined within the boundaries of the 1-cut-wire metasurface transverse to the propagation direction of the SSPP, as the mode profile in the bottom row of Fig. 8(a) confirms. The slight deviation between the measured and simulated mode profile can be explained by the limited 50 µm x 50 µm spatial resolution of the near-field measurement. For the same reason, the agreement between the measured and simulated mode profile improves, when the SSPP mode distribution spatially widens for an increasing number of cut wires (see bottom row of Figs. 8(b) and 8(c)). Below a frequency of 0.48 THz, no SSPP propagation is observed, in accordance with the eigenmode solutions that predict a low SSPP cut-off frequency of 0.48 THz. According to the calculated dispersion relation, the SSPPs propagate with subwavelength confinement to the surface at frequencies above 0.48 THz. For confirmation, we analyzed the measured SSPP near-field at 0.54 THz. Compared to the SSPP propagation at the low cut-off-frequency, we recognized a decrease in the propagation length of the SSPPs that goes along with a stronger attenuation of the SSPP near-field along the propagation path. This is expected, since a stronger confinement of the SSPPs to the surface implies an increased loss in the metal and in the dielectric of the metasurface. Furthermore, the measured electric field amplitude decreases, when the SSPP frequency increases and approaches the high cut-off-frequency of the considered SSPP mode. This behavior can also be attributed to an increased confinement of the SSPP mode in the area close to the metasurface.

The same qualitative behavior can be confirmed for the propagation of SSPP modes on a straight 2- and 3-cut-wire metasurface, as shown in Figs. 8(b) and 8(c). From the 2-D near field scans, we determined low cut-off frequencies of 0.32 THz for the 2-cut-wire metasurface and 0.29 THz for the 3-cut-wire metasurface. As for the 1-cut-wire metasurface, the measured electric field amplitude decreases for monotone increase of the SSPP frequency towards the high-cut-off frequency. At the same time, the attenuation of the SSPP along the propagation path increases due to increasing loss in the metal and dielectric of the metasurface, which implies a drop in the propagation length. Again, both observations point at a growing confinement of the SSPPs in the direction normal to the surface, when the SSPP frequency increases towards the high cut-off frequency. In comparison to the narrow 1-cut-wire metasurface, the electric field distribution of the SSPP mode spreads transverse to its propagation direction for increasing path width. Yet, the SSPP mode remains tightly confined within the transverse path boundaries. As for the 1-cut-wire metasurface, the SSPP mode on the 2- and 3-cut-wire metasurface is anti-symmetric with respect to an axis through y = 1000µm parallel to the x-axis. In agreement with the numerical simulation of the electric near-field distribution of the SSPPs, the minimum of the E_z-field in the transverse center of the anti-symmetric SSPP mode becomes more pronounced and wider for increasing path width, since the SSPP near-field is strongly enhanced at the outer transverse boundaries. This behavior can be clearly observed, when we compare the SSPP electric fields on a 2-cut-wire metasurface at 0.42 THz (Fig. 8(b)) and on a 3-cut-wire metasurface at 0.36 THz (Fig. 8(c)). In this comparison, the frequencies were selected to be well located in the frequency range, for which we expect subwavelength confinement of the SSPPs to the metasurfaces. It should be noted that the unbalanced field amplitude distribution and the slight horizontal deviation of the propagation direction of the anti-symmetric SSPP mode in Fig. 8(c) is an artifact that was caused by an undesired tilt of the flexible substrate of the metasurface.

For experimental evaluation of the dispersion relation of the SSPPs on the fabricated metasurfaces, we determined the wavelength of the propagating SSPP mode as a function of the frequency. For this purpose, we evaluated snapshots of the spatial electric field distribution of the SSPPs for different frequencies. By determination of the spatial locations of the maxima and minima of the real part of the measured electric SSPP field on a line in the direction of the SSPP propagation, we determined the wavelength λ of the SSPP mode at three different frequencies for each metasurface. For the straight 1-, 2- and 3-cut-wire metasurface, the upper three rows of Figs. 9(a)

Optics EXPRESS

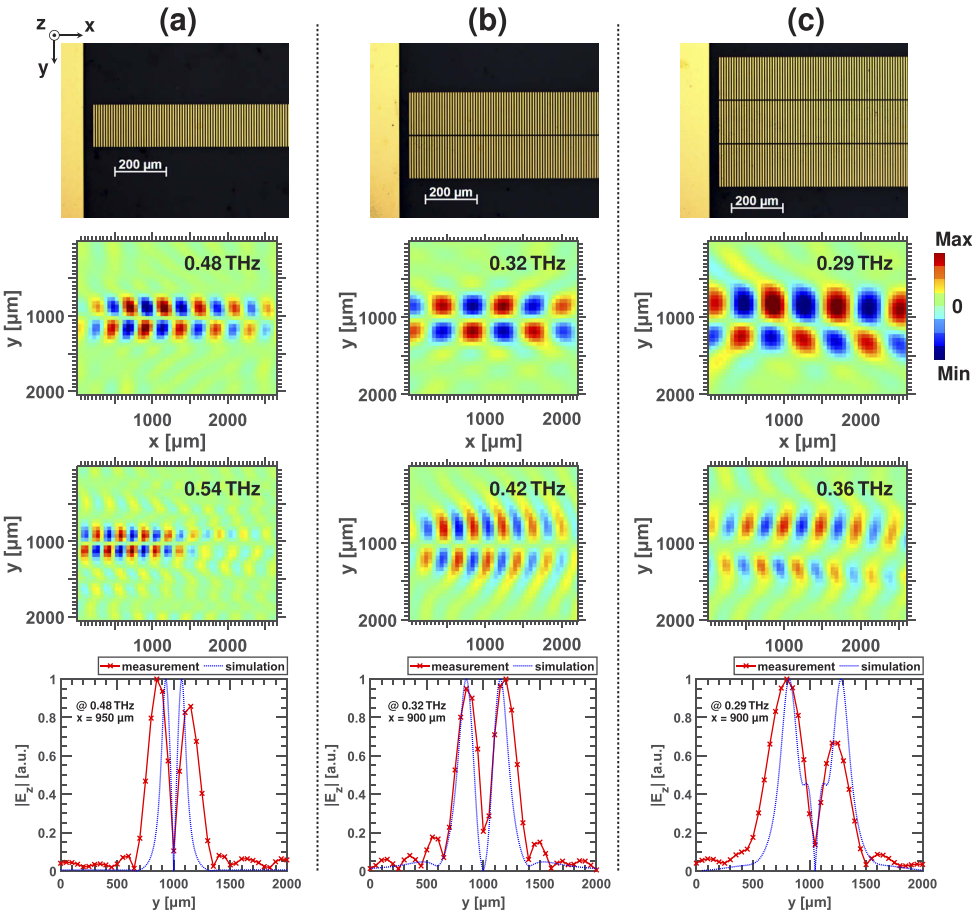

Fig. 8. For each column (a) to (c), the rows contain from top to bottom: a microscope image of the investigated metasurface together with two snapshots of the spatial distribution of the SSPP electric field, one measured at the low SSPP cut-off frequency and the other measured for a frequency above the SSPP cut-off frequency, The graphs in the bottom row show a comparison between the measured and numerically simulated electric field distribution of the SSPPs along an intersection line in y-direction.

to 9(c) show the snapshots of the real part of the SSPP electric field at the three evaluation frequencies. Additionally, the bottom row of Figs. 9(a) to 9(c) display a plot of the numerically calculated dispersion relation together with the experimentally determined dispersion points at the three evaluation frequencies. With the relation $k_x = 2\pi/\lambda$, we converted the measured SSPP wavelength into the wavenumber in order to plot these points in the corresponding dispersion diagram in the bottom rows of Figs. 9(a) to 9(c). The experimentally determined dispersion at the three different evaluation frequencies and the snapshot graphs, from which we derived the dispersion points, are related by their colors. In the dispersion diagram, we also plotted the light line of free space and the light line of the dielectric substrate. As can be seen, the measured dispersion at the three evaluation frequencies lies on the numerically calculated dispersion curve for all three metasurfaces. This is a further confirmation that the measured behavior of the experimentally investigated SSPP modes is in good agreement with the predictions of the numerical calculations.

Optics EXPRESS

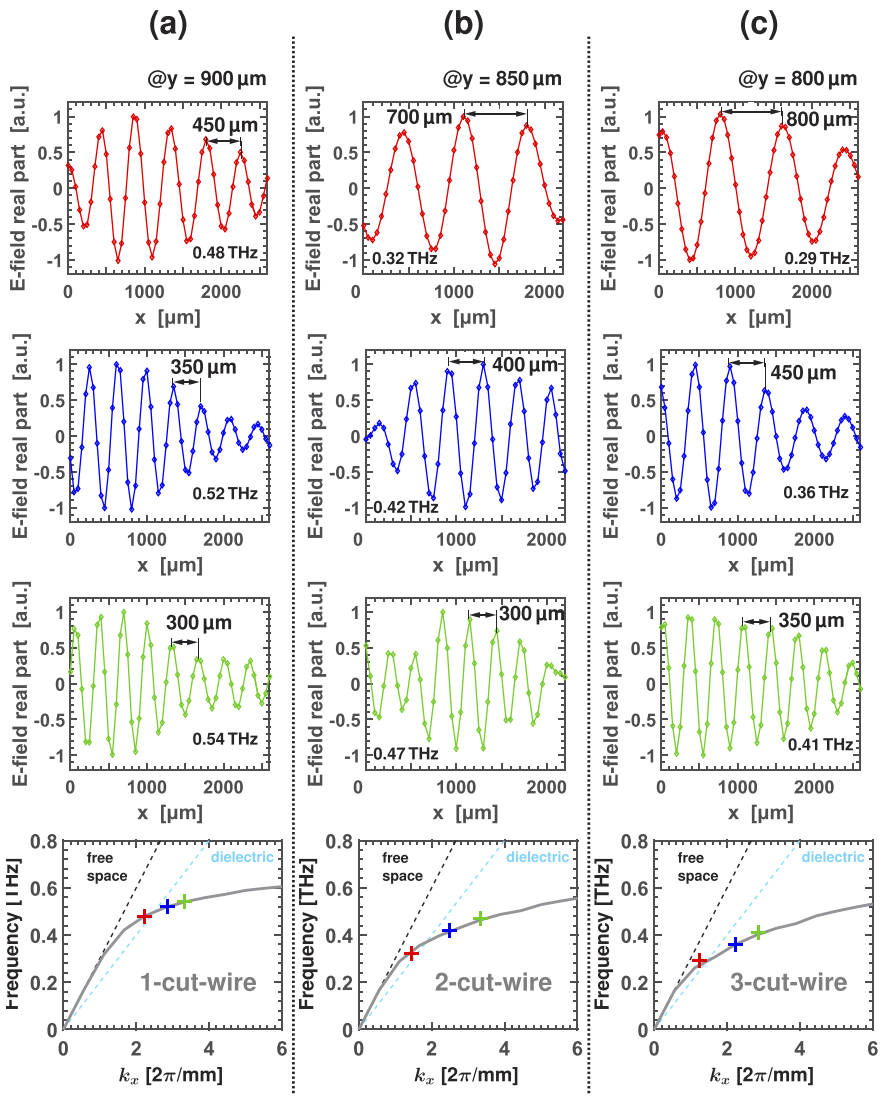

Fig. 9. The graphs in columns (a) to (c) show the results of the measured electric field distribution and the measured dispersion for SSPPs that travel on (a) a 1-cut-wire, (b) a 2-cut-wire, and (c) a 3-cut-wire metasurface along a straight pathway in x-direction. In more detail, the upper three rows of each column ((a)–(c)) depict graphs of the real part of the measured electric SSPP field as a function of the position x in the propagation direction of the SSPP. In the bottom row of each column, the numerically calculated dispersion of the SSPP is plotted as a gray curve together with the light line of free space (black dashed) and the light line of the dielectric substrate (blue dashed). For comparison, the experimentally measured dispersion points of the SSPPs are plotted for three different frequencies. The wavelength and the wavenumber of the SSPP mode was determined from the measured electric SSPP field distributions in the corresponding three top rows.

In an additional experiment, we investigated the possibility to route SSPPs along a given path on the metasurface. As explained earlier, we designed and fabricated a metasurface that is composed of 3 cut-wires in the direction transverse to the propagation direction and whose outline of the outer boundaries describes a 90° curve. In order to prove proper routing of the

Optics EXPRESS

confined SSPPs within the propagation plane, we imaged the electric near-field of the SSPPs under the same experimental conditions as for the the metasurfaces with straight pathways. Figure 10(a) shows a microscope picture of the curved 3-wire-metasurface path. A color map of the measured spatial distribution of the real part of the electric near-field of the SSPPs is plotted in Fig. 10(b) in comparison to the corresponding numerically calculated field distribution in Fig. 10(c). For visualiation of the geometric relation between the SSPP field distribution and the metasurface, the corresponding metasurface structure is outlined underneath the E-field plot in Fig. 10(c). As expected from the numerical simulations in Fig. 10(c), the measurements in Fig. 10(b) confirm a subwavelength confinement of the SSPPs within the boundaries of the pathway during propagation. Since the metasurface concurrently supports a subwavelength field confinement of the SSPPs in the direction normal to the surface, the use of metasurface pathways provides us with proper means to guide terahertz waves along pre-defined routes, while a subwavelength confinement within the in-plane boundaries is maintained.

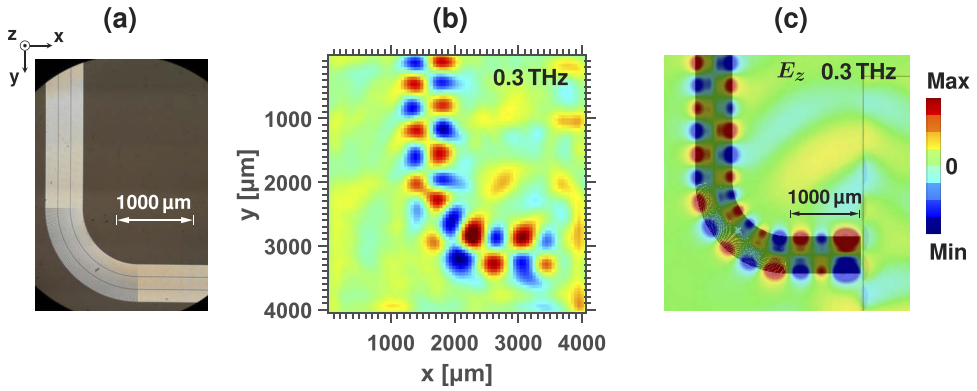

Fig. 10. (a) Microscope image of a 3-cut-wire metasurface along a curved pathway. (b) Color map of the real part of of the z-component of the measured electric SSPP field along a curved pathway at a frequency of 0.3 THz. (c) Numerically calculated real part of the z-component of the electric field. The field was monitored in the *xy*-plane at a distance of 50µm from the metasurface at a frequency of 0.3 THz. The metasurface structure is visualized underneath the field distribution together with the outline of the metal patch at the right side of the view graph.

5. Conclusion

We studied the propagation of strongly confined terahertz surface plasmon polaritons (SSPPs) along straight and curved pathways of subwavelength width on specifically designed metasurfaces. The metasurface paths were composed of cut-wire unit cells on a dielectric thin-film substrate. We numerically calculated the dispersion of the SSPP mode and simulated the propagating electromagnetic fields of the SSPPs on the metasurfaces. We observed that the designed metasurface guides the SSPPs on pathways with subwavelength width. Over the full propagation length, the SSPPs additionally display a subwavelength confinement in the direction normal to the metasurface. These findings hold true for both, the propagation on straight routes and the propagation on curved courses. We recognized that a narrowing of the path width results in a reduced spectral bandwidth of the SSPP mode. For experimental verification, we fabricated metasurfaces containing straight paths with a width of 1, 2 and 3 cute-wire unit cells as well as a metasurface embodying a curved pathway with a width of 3 cut-wire unit cells. The SSPP mode was excited by edge coupling of terahertz waves from a metal patch. The electric field of the SSPPs was measured by use of a near-field imaging terahertz spectroscope. In the experiments,

Optics EXPRESS

we confirmed the propagation of SSPPs along straight and curved routes with propagation lengths of several millimeters. The SSPPs were tightly confined to the surface and limited to a subwavelength scale by the path width of the metasurface structures. We verified that the experimentally observed SSPP mode displayed the same spectral dispersion as in the numerical calculations. Furthermore, the experiment affirmed that a reduction of the path width decreases the spectral bandwidth of the SSPP mode. This underscores that the path width is a crucial quantity for proper routing of SSPPs on metasurfaces, and thus plays an important role for the design and implementation of terahertz integrated circuits.

Funding

Deutsche Forschungsgemeinschaft (RA 1903/4-1).

Disclosures

The authors declare no conflicts of interest.

References

1. S. Maier, *Plasmonics: Fundamentals and Applications* (Springer, 2007).
2. P. Berini, "Plasmon-polariton modes guided by a metal film of finite width bounded by different dielectrics," Opt. Express **7**(10), 329–335 (2000).
3. J. T. Kim, J. J. Ju, S. Park, M.-s. Kim, S. K. Park, and M.-H. Lee, "Chip-to-chip optical interconnect using gold long-range surface plasmon polariton waveguides," Opt. Express **16**(17), 13133–13138 (2008).
4. R. Charbonneau, N. Lahoud, G. Mattiussi, and P. Berini, "Demonstration of integrated optics elements based on long-ranging surface plasmon polaritons," Opt. Express **13**(3), 977–984 (2005).
5. R. Méjard, J. Dostálek, C.-J. Huang, H. Griesser, and B. Thierry, "Tuneable and robust long range surface plasmon resonance for biosensing applications," Opt. Mater. **35**(12), 2507–2513 (2013).
6. B. You, C.-C. Peng, J.-S. Jhang, H.-H. Chen, C.-P. Yu, W.-C. Lai, T.-A. Liu, J.-L. Peng, and J.-Y. Lu, "Terahertz plasmonic waveguide based on metal rod arrays for nanofilm sensing," Opt. Express **22**(9), 11340–11350 (2014).
7. B. You, J.-Y. Lu, T.-A. Liu, and J.-L. Peng, "Hybrid terahertz plasmonic waveguide for sensing applications," Opt. Express **21**(18), 21087–21096 (2013).
8. O. Krupin, H. Asiri, C. Wang, R. N. Tait, and P. Berini, "Biosensing using straight long-range surface plasmon waveguides," Opt. Express **21**(1), 698–709 (2013).
9. J. B. Pendry, L. Martín-Moreno, and F. J. Garcia-Vidal, "Mimicking surface plasmons with structured surfaces," Science **305**(5685), 847–848 (2004).
10. Z. Gao, L. Wu, F. Gao, Y. Luo, and B. Zhang, "Spoof plasmonics: From metamaterial concept to topological description," Adv. Mater. **30**(31), 1706683 (2018).
11. T. Fip, B. Reinhard, J. Neu, and M. Rahm, "Metamaterial-mediated terahertz surface waves with strong confinement," in "*2013 38th International Conference on Infrared, Millimeter, and Terahertz Waves (IRMMW-THz)*," (2013), pp. 1–2.
12. B. Reinhard, O. Paul, R. Beigang, and M. Rahm, "Experimental and numerical studies of terahertz surface waves on a thin metamaterial film," Opt. Lett. **35**(9), 1320–1322 (2010).
13. S. Becker, T. Fip, C. Shemelya, and M. Rahm, "Confined terahertz surface waves on meta-surfaces and goubau lines," in "*SPIE Nanoscience + Engineering*," vol. 10719 (SPIE, 2018), p. 7.
14. X. Liu, Y. Feng, K. Chen, B. Zhu, J. Zhao, and T. Jiang, "Planar surface plasmonic waveguide devices based on symmetric corrugated thin film structures," Opt. Express **22**(17), 20107–20116 (2014).
15. X. Gao, L. Zhou, and T. J. Cui, "Odd-mode surface plasmon polaritons supported by complementary plasmonic metamaterial," Sci. Rep. **5**(1), 9250 (2015).
16. S. Sun, Q. He, S. Xiao, Q. Xu, X. Li, and L. Zhou, "Gradient-index meta-surfaces as a bridge linking propagating waves and surface waves," Nat. Mater. **11**(5), 426–431 (2012).
17. M. Navarro-Cía, M. Beruete, S. Agrafiotis, F. Falcone, M. Sorolla, and S. A. Maier, "Broadband spoof plasmons and subwavelength electromagnetic energy confinement on ultrathin metafilms," Opt. Express **17**(20), 18184–18195 (2009).
18. W. Zhang, G. Zhu, L. Sun, and F. Lin, "Trapping of surface plasmon wave through gradient corrugated strip with underlayer ground and manipulating its propagation," Appl. Phys. Lett. **106**(2), 021104 (2015).
19. Y. Meng, H. Ma, J. Wang, Y. Lv, M. Feng, Z. Li, and S. Qu, "Dispersion engineering of metasurfaces for supporting both tm and te spoof surface plasmon polariton," J. Phys. D: Appl. Phys. **51**(4), 045109 (2018).
20. L. Ye, W. Zhang, B. K. Ofori-Okai, W. Li, J. Zhuo, G. Cai, and Q. H. Liu, "Super subwavelength guiding and rejecting of terahertz spoof spps enabled by planar plasmonic waveguides and notch filters based on spiral-shaped units," J. Lightwave Technol. **36**(20), 4988–4994 (2018).

Optics EXPRESS

21. Y. J. Guo, K. Da Xu, and X. Tang, "Spoof plasmonic waveguide developed from coplanar stripline for strongly confined terahertz propagation and its application in microwave filters," Opt. Express **26**(8), 10589–10598 (2018).
22. L. Ye, Y. Xiao, N. Liu, Z. Song, W. Zhang, and Q. H. Liu, "Plasmonic waveguide with folded stubs for highly confined terahertz propagation and concentration," Opt. Express **25**(2), 898–906 (2017).
23. I. R. Hooper, B. Tremain, J. A. Dockrey, and A. P. Hibbins, "Massively sub-wavelength guiding of electromagnetic waves," Sci. Rep. **4**(1), 7495 (2015).
24. X. Shen, T. J. Cui, D. Martin-Cano, and F. J. Garcia-Vidal, "Conformal surface plasmons propagating on ultrathin and flexible films," Proc. Natl. Acad. Sci. U. S. A. **110**(1), 40–45 (2013).
25. D. Zhang, K. Zhang, Q. Wu, R. Dai, and X. Sha, "Broadband high-order mode of spoof surface plasmon polaritons supported by compact complementary structure with high efficiency," Opt. Lett. **43**(13), 3176–3179 (2018).
26. S. A. Maier, S. R. Andrews, L. Martín-Moreno, and F. J. García-Vidal, "Terahertz surface plasmon-polariton propagation and focusing on periodically corrugated metal wires," Phys. Rev. Lett. **97**(17), 176805 (2006).
27. M. Islam, D. R. Chowdhury, A. Ahmad, and G. Kumar, "Terahertz guided mode properties in an internally corrugated plasmonic waveguide," J. Appl. Phys. **122**(5), 053105 (2017).
28. G. Kumar, S. Pandey, A. Cui, and A. Nahata, "Planar plasmonic terahertz waveguides based on periodically corrugated metal films," New J. Phys. **13**(3), 033024 (2011).
29. W. Zhu, A. Agrawal, and A. Nahata, "Planar plasmonic terahertz guided-wave devices," Opt. Express **16**(9), 6216–6226 (2008).
30. D. Guan, P. You, Q. Zhang, K. Xiao, and S. Yong, "Hybrid spoof surface plasmon polariton and substrate integrated waveguide transmission line and its application in filter," IEEE Trans. Microwave Theory Tech. **65**(12), 4925–4932 (2017).
31. C. R. Williams, S. R. Andrews, S. A. Maier, A. I. Fernández-Domínguez, L. Martín-Moreno, and F. J. García-Vidal, "Highly confined guiding of terahertz surface plasmon polaritons on structured metal surfaces," Nat. Photonics **2**(3), 175–179 (2008).
32. Y. Zhang, Y. Xu, C. Tian, Q. Xu, X. Zhang, Y. Li, X. Zhang, J. Han, and W. Zhang, "Terahertz spoof surface-plasmon-polariton subwavelength waveguide," Photonics Res. **6**(1), 18–23 (2018).
33. D. Martin-Cano, M. L. Nesterov, A. I. Fernandez-Dominguez, F. J. Garcia-Vidal, L. Martin-Moreno, and E. Moreno, "Domino plasmons for subwavelength terahertz circuitry," Opt. Express **18**(2), 754–764 (2010).
34. J. Neu, B. Krolla, O. Paul, B. Reinhard, R. Beigang, and M. Rahm, "Metamaterial-based gradient index lens with strong focusing in the thz frequency range," Opt. Express **18**(26), 27748–27757 (2010).